Bulletin of the Seismological Society of America, 91, 6, pp. 1820–1830, December 2001

Shallow Seismic Profiling of the Exhumed Punchbowl Fault Zone, Southern California

by Yong-Gang Li, Frederick M. Chester, and John E. Vidale

Abstract The relationship between seismic velocity and internal fault structure was investigated through a shallow seismic refraction experiment across the Punchbowl fault, Devil's Punchbowl Los Angeles County Park, California. The Punchbowl fault is a northwest-striking, large-displacement fault of the San Andreas system that is exhumed to several kilometers depth and places crystalline basement against arkosic sandstone of the Punchbowl Formation. Seismic refraction profiles using hammer and impulsive shear-wave sources along a 300-m-long line reveal the velocity structure of the fault zone beneath a thin deposit of alluvium. We determine a velocity model assuming the alluvial layer is fairly uniform in velocity and thickness consistent with geologic observations and *P*-wave travel times. Raytracing with damped least-squares inversion of travel times of *P* and *S* waves indicate that the Punchbowl fault is best modeled as a zone several tens of meters wide with velocities reduced by 10%–25% from wall-rock velocities (V_p = 3.2 km/sec for granitic basement and V_p = 2.9 km/sec for Punchbowl Formation). Thickness of the low-velocity zone and the variation in seismic velocity across the zone are qualitatively consistent with expectations based on the observed distribution of fault-related fracturing and alteration. Apparent crack densities calculated from measured seismic velocities using O'Connell and Budiansky (1974) formulation for a cracked medium range from about 0.4 in the core to a background crack density of 0.1 in the host rock. The variation in calculated crack density across the fault is similar to observed variations in microfracture density in the Punchbowl Formation sandstone along traverses across the fault. An estimate of the Poisson's ratio near the fault is about 0.25, suggesting that open cracks in the shallow part of the Punchbowl fault zone are dry, consistent with the geologically inferred location of the groundwater table. Although the seismic data do not completely constrain the velocity structure, the seismic velocity model determined by raytracing and inversion of travel times is admissible on the basis of structural data.

Introduction

A refined definition of the internal structure of fault zones in the seismogenic portion of the continental crust is necessary to further our understanding of the processes of earthquake rupture initiation, propagation, and termination. Images of seismogenic fault zones at depth have been produced using seismic tomography (Aki and Lee, 1976; Thurber, 1983; Lees and Malin, 1990; Michelini and McEvilly, 1991; Eberhart-Phillips and Michael, 1993) and by observations and modeling of fault-zone trapped waves (Li *et al.,* 1990, 1994, 2000; Leary *et al.,* 1991; Hough *et al.,* 1994). These studies have shown that faults are marked by low-velocity zones of tabular geometry. Fault-zone trapped waves suggest that the large-displacement faults of the San Andreas system are characterized by zones on the order of 100 to 200 m thick with average seismic velocity of approximately 30%–40% of the surrounding host rock. On the basis of geologic studies of fault internal structure, the fault-related low-velocity zones are thought to reflect mineralogic alteration and intense fracturing associated with faulting (Sibson, 1977; Mooney and Ginzburg, 1986).

Geologic study of earthquake rupture zones (Sieh *et al.,* 1993; Johnson *et al.,* 1994) and of exhumed faults (Chester and Logan, 1986; Chester *et al.,* 1993; Schulz and Evans, 1998) document that fault displacements often are localized to a narrow fault core, but that fault-related fractures and other deformation occur over a broader damage zone. In the Punchbowl and San Gabriel faults, which are exhumed faults of the San Andreas system in southern California, fracture

density decreases exponentially with distance from the fault core (Chester and Logan, 1986). In these two fault zones, fracture density within tens of meters of the fault core is significantly greater than the regional level density.

A combined seismic and structural geology study of a fault zone would help in determining if seismic velocity variation and fracture density distributions are correlated. This article presents the results from a shallow refraction experiment to measure compression and shear-wave velocity across the Punchbowl fault at a location near which the internal structure of the fault zone is well characterized at both the macroscopic and microscopic scales. We found a good correlation between the changes in seismic velocity and fracture density along traverses across the fault zone.

Geology of the Punchbowl Fault

The Punchbowl fault is an inactive, exhumed fault of the San Andreas transform system in the central Transverse Ranges of southern California (Fig. 1). The Punchbowl fault was active during the Miocene–Pliocene and accommodated approximately 45 km of the right-lateral strike-slip displacement (Dibblee, 1968; Weldon *et al.,* 1993). On the north side of the San Gabriel Mountains in the Devil's Punchbowl Los Angeles County Park, the fault was eroded to low relief in Pleistocene time and covered by Quaternary piedmont alluvial fans after it became inactive (Dibblee, 1987). Recent uplift has rejuvenated erosion to dissect the piedmont and has exposed the Punchbowl fault and associated folds. As a result, the fault zone is extremely well exposed in canyons of drainage crossing the fault. Previous studies have concluded that the fault is exhumed to 2- to 4-km depth on the basis of stratigraphic relations, microstructures, and mineral assemblages of the fault rocks (Chester and Logan, 1986).

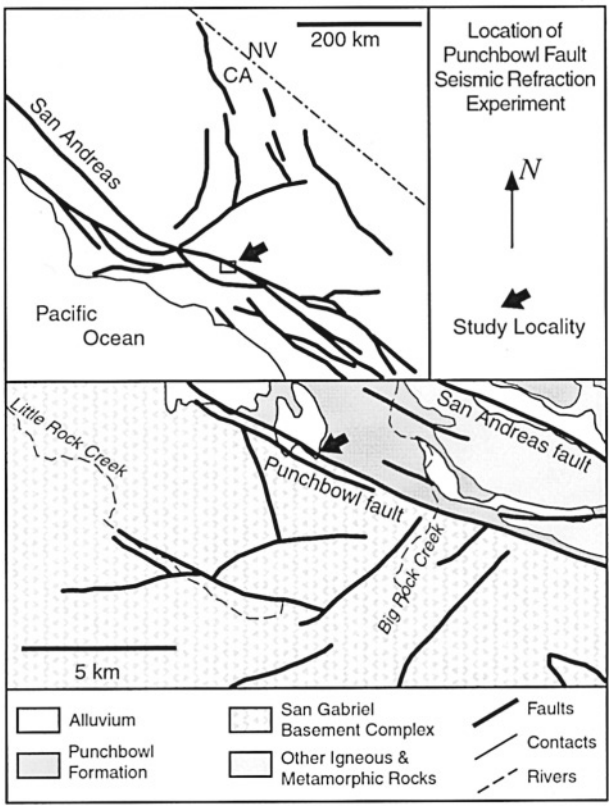

Figure 1. Location of the Punchbowl fault in the San Gabriel Mountains, southern California. In the Devil's Punchbowl Los Angeles County Park, California, the Punchbowl fault juxtaposes arkosic sandstone and mudstone of the Punchbowl Formation and the crystalline basement complex of the San Gabriel Mountains.

In the Devil's Punchbowl area, the Punchbowl fault system consists of the northernmost and southernmost principal faults that bound a slice of fractured and faulted basement up to 0.5 km in width (Fig. 1). The slice of fractured basement contains heterogeneous assemblage of granitic and gneissic rocks that have been mineralogically altered and deformed to varying degrees (Cox *et al.,* 1983). The northern fault strand, the Punchbowl fault, is better developed and places the cataclastically deformed basement rock against arkosic sedimentary rocks of the Punchbowl Formation along a single, continuous, ultracataclasite layer (Fig. 2). The southern fault strand is segmented and not as well developed. Previous structural mapping indicated that nearly all of the displacement on the Punchbowl fault system was localized to the ultracataclasite layer of the northern fault strand (Chester and Chester, 1998).

The Punchbowl fault consists of a broad zone of damaged rock bounding a several-meters-thick core of cataclastically deformed rock containing a continuous ultracataclasite layer along which the Punchbowl Formation sandstone and basement complex are juxtaposed. The average orientation of the ultracataclasite layer is N70°W and dips steeply 75° to the southwest (Fig. 2b). Fabric analyses indicate that the Punchbowl fault is a right-lateral oblique-reverse-slip fault with the slip vector plunging approximately 30° to the southeast (Chester and Logan, 1987). Measurements of mesoscopic scale fracture density and microfracture density in the sandstone indicate highly fractured rock near the ultracataclasite layer and a decrease in density to regional levels at a distance of about 50 m (Chester and Logan, 1986; Wilson *et al.,* 1999). A similar variation in fracture density with distance from the ultracataclasite layer occurs in the basement rocks as well (Schulz and Evans, 1998). Subsidiary fault and microfracture fabrics along the Punchbowl fault are consistent with progressive accumulation of damage throughout the faulting history. Within the damaged zone, the preferred orientation of microfractures is nearly normal to the fault. Both microfractures and subsidiary fault fabrics are consistent with a maximum principal compressive stress at large angles to the ultracataclasite layer at the time of fracture and fault formation. Within the meters-thick fault core, subsidiary faults and fractures display an additional preferred orientation approximately parallel to the fault, consistent with the extremely large shear strain in the core.

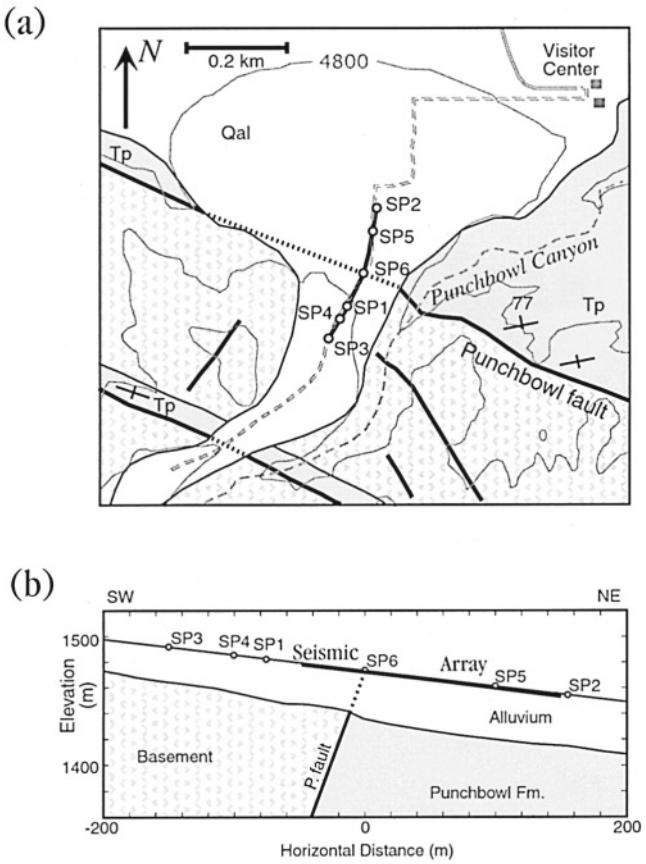

Figure 2. (a) Location of the refraction profile with six source points (SP) along a jeep trail across the Punchbowl fault southwest of the Devil's Punchbowl Park Visitor Center. The seismic profile is on an uplifted alluvial surface and oriented approximately perpendicular to the strike of the Punchbowl fault. Source point SP6 is located at the inferred surface projection of the Punchbowl fault, and serves as the origin (0 m) for measuring distance along the seismic profile, where positive distance is to the northeast. The 195-m-long seismic array is shown by the thick solid line. The spacing of elevation contour lines is 200 ft. Outcropping Punchbowl Formation is marked by the stippled pattern labeled Tp, alluvium is white and labeled Qal, and the unlabeled stippled pattern marks crystalline basement. The dotted line is the interpolation between the explosures of the Punchbowl fault in the canyons to the southeast and to the northwest. The strike and dip symbols are printed. (b) Geologic structure below the refraction profile between SP3 and SP2 interpreted from geologic map and outcrop relations. The dotted line is interpreted as the projection of the Punchbowl fault to surface.

Seismic Refraction Experiment

The seismic refraction profiling experiment was conducted across the Punchbowl fault (i.e., the northern fault of the Punchbowl fault system) on the west of the Devil's Punchbowl Los Angeles County Park. The profile is oriented approximately perpendicular to the fault and is sited along a jeep trail on the piedmont alluvial fan surface (Fig. 2a). The inclination of the surface along the jeep trail is about 7° to the north. The ground surface is very smooth at the site. The seismic profiles shown below also indicate a gentle base of alluvium. Although the fault is covered by Quaternary alluvial deposits, the point where the projection of the fault surface crosses the jeep trail (Fig. 2b) could be located to within ± 10 m on the basis of fault expressions in the canyons a few hundred meters to the southeast and the northwest (Fig. 2a). The ultracataclasite layer of the fault is exposed in the Punchbowl Canyon about 150 m east and in a small drainage about 250 m west of the jeep trail. We estimate that the thickness of alluvium overlying the bedrock at the seismic profiling site is approximately 30–40 m, based on the topography of bedrock outcrops east and west of the jeep trail (Fig. 2a). It would have been ideal to site the seismic profile directly on bedrock; however, it was not feasible to conduct the experiment in sites where the bedrock is exposed in the canyons because of the locally rough topography and inaccessibility.

The seismic refraction profile was conducted with a PASSCAL 60-channel 24-bit GEOMETRICS StrataView Exploration seismograph connected to 20 three-component L22 sensors (Mark Products) via a 100-m-long cable with station spacing of 5 m. The cable was moved along the jeep trail to form the total array length of 195 m (Fig. 2b). Three components of sensors were aligned vertical, parallel, and perpendicular to the seismic line. The array crosses the inferred surface projection of the Punchbowl fault at a distance of 45 m from the southwestern end of the array.

We used a sledgehammer source at six points (SP1-6) and an air-powered impact shear-wave source of the U.S. Geological Survey (USGS) at two points (SP1 and SP2) on the seismic line to generate seismic signals for the study of the compressional and shear-wave structure. Source points SP1, SP4, and SP3 were located at 75, 100, and 150 m southwest of the inferred fault trace, whereas source points SP5 and SP2 were located at 100 and 155 m northeast of the trace, respectively (Fig. 2). Source point SP6 was positioned on the inferred surface projection of the fault. At each source point, we hit the hammer on a metal plate on the ground at least 40 times. The shear source provided by H. P. Liu of the USGS (Liu *et al.,* 1996) was operated with the air-powered sliding metal mass in the direction perpendicular to the seismic line. By differencing the shear source operating with both polarities, we generated nearly pure *SH* waves. We repeated the signal at least 30 times in each polarization direction at SP1 and SP2. The dominant frequencies of hammer-generated signals are between 40 and 80 Hz, whereas the dominant frequencies of signals recorded for the shear-wave source are 30–60 Hz. Signals were recorded at the rate of 2000 samples/sec. The recorder was triggered by the signal from an acceleration sensor taped on the hammer or on the horizontal metal beam of the shear-wave source. The repeated signals from each source point were stacked in

the internal memory of Geometrics recorder to enhance the signal-to-noise ratio.

Figure 3a illustrates refraction profiles on the 195-m-long seismic array across the Punchbowl fault for the sledge hammer applied at SP1 and SP2, respectively. SP1 and SP2 were located 75 m southwest and 155 m northeast of the inferred surface projection of the fault. The direct *P* waves are prominent in the parallel-to-line component seismograms, whereas the refracted *P* waves are prominent in the vertical component seismograms. The direct *P* waves traveled in the piedmont alluvial layer. The refracted *P* waves were from the interface between the alluvium and bedrock. The refracted waves from SP2 passed the fault zone in bedrock, but the refracted waves from SP1 did not because the critical distance for refracted waves was beyond the distance between SP1 and the inferred position of the fault. The alignments of direct *P* waves from either SP1 or SP2 are nearly straight, indicating a homogeneous alluvial fan overlying the bedrock at the site. The compressional velocity of the alluvium is estimated to be about 1.0 km/sec. The alignment of refracted *P* waves from SP1 is also nearly straight, showing a low relief base of the alluvium on the bedrock southwest of the fault. However, the alignment of refracted *P* waves from SP2 shows a time delay at stations close to the inferred position of the Punchbowl fault, probably because of the lower velocity of the fault zone in the bedrock. The compressional velocity at the surface of the bedrock is estimated to be about 2.5–3.3 km/sec near the fault. Taking compressional velocity $V_a = 1$ km/sec for the alluvium and $V_b = 3$ km/sec for the bedrock, and the interception time $t_0 = 75$ msec for refracted *P* waves, we estimated the thickness h of the alluvium layer overlying the bedrock to be about 40 m using the equation $h = V_a t_0 / 2\cos i$ where $i = \sin^{-1}(v_a/v_b)$. This thickness of the alluvial layer is consistent with that estimated from geologic mapping.

The *SH* waves generated by the air-powered impulsive *SH* source at SP1 and SP2 and recorded at the array (Fig. 3b) show similar features as those for *P* waves. The ratio of travel times of either direct or refracted *P* to *SH* waves in profiles is about 0.6, suggesting that the rock near the Punchbowl fault at shallow depth is nearly Poissonian.

Figure 4 illustrates the refraction profiles on the southwest half of the seismic array, which covered the inferred position of the fault, for the hammer source at SP3 and SP5 located 150 m southwest and 100 m northeast of the inferred position of the Punchbowl fault. The direct and refracted *P* waves appeared clearly in the parallel-to-line component and the vertical component seismograms, respectively. The alignments of direct *P* waves from both source points are straight, showing again a uniform alluvium at the site. The alignment of refracted *P* waves from SP5 is straight, showing a flat base of the alluvium on bedrock northeast of the fault. However, refracted *P* waves at stations close to the inferred fault for SP3 show a slight time delay, probably caused by the lower-velocity fault zone in the bedrock.

Multiple bandpass-filtered surface waves from the *SH* source (Fig. 5) further show that the alluvial layer overlying the bedrock at the profiling site is quite uniform. We used a narrow bandpass filter with a bandwidth of 2 Hz and centered at the frequencies of 10, 15, and 20 Hz. Multiple bandpass-filtered *SH* component seismograms show the dispersion of the Love-type surface waves between 10 and 20 Hz. The Love waves at 10 Hz show a coherent phase, whereas those waves at 20 Hz have some shingling. Observations of surface waves suggest a quite homogeneous alluvial layer with the thickness of at least 25 m overlying bedrock at the site.

The Velocity Model and Calculated Crack Density

We manually picked arrival times of direct and refracted *P* and *S* waves from six seismic profiles across the Punchbowl fault. When the signal-to-noise ratio in seismograms was higher than 4, the error in picked arrival times was lesser than 2 msec (four samples) for *P* waves and lesser than 3 msec (six samples) for the *S* waves. If the signal-to-noise ratio was lower than 4, we used cross correlation to measure the time shift between arrivals at two neighboring stations. Because the *SH* source generated nearly pure *SH* motions, the affect of *P* coda on the pick of *S* arrivals was reduced significantly. However, the onsets of refracted *S* waves were not as sharp as the onsets of refracted *P* waves, perhaps because of the *S* to *P* conversion on the fractured anisotropic rocks. The picked travel times of *P* and *S* waves for six source points (SP1-6) were used for raytracing modeling.

We then constructed a structural velocity model across the Punchbowl fault for raytracing (Fig. 6a). The model includes an alluvial layer overlying the bedrock cut by the Punchbowl fault. The alluvial layer is assumed to be laterally homogeneous, with a slight vertical velocity gradient. A low-velocity fault zone is assumed to be sandwiched between the fractured granitic bedrock to the southwest and the sandstone of Punchbowl Formation to the northeast.

We used a 2D raytracing code with the damped least-squares inversion procedure (Zelt and Smith, 1992) to analyze travel times of *P* and *S* waves. The grid spacing in the model was not even. We used 5–10 m spacing for grids close to the fault but larger spacing for grids farther away from the fault. The fault was placed at 0 m, in the middle of the model. For raytracing of *S* waves, we specified a Poisson's ratio by which the *P* velocity was converted to *S* velocity at each grid. We generated synthetic travel times of *P* waves for six hammer source points (SP1-6) and travel times of *S* waves for two *SH* source points (SP1, 2).

In the first step of modeling, we used a flat interface between the alluvial layer and bedrock. We specified *P*-wave velocities at grids above and below the layer interface in the model. The velocities in the alluvial layer were constrained by travel times of direct waves, whereas the depth and velocities of bedrock were mainly constrained by travel times of refracted waves. In the second step of modeling, we fixed velocities of the alluvial layer but let the velocities and the

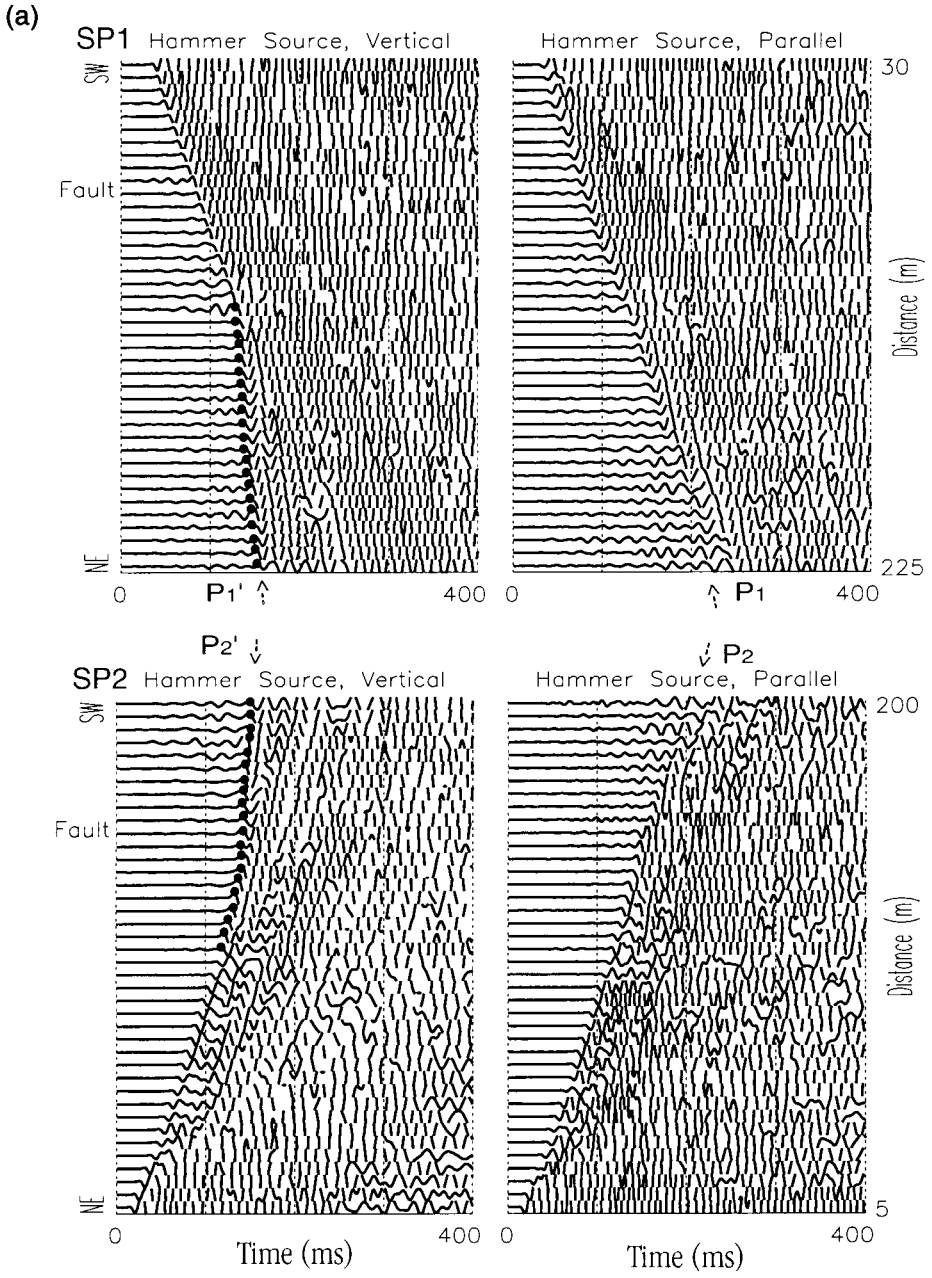

Figure 3. (a) Refraction profiles on a 195-m-long seismic array across the Devil's Punchbowl fault using the sledge hammer at source points (top) SP1 and (bottom) SP2, located 75 m southwest and 155 m northeast of the inferred surface projection of the Punchbowl fault (denoted by Fault), respectively. Distances between the source points and the ends of seismic array are plotted at right. The station spacing of the array is 5 m. The vertical and parallel-to-array component seismograms are displayed. Seismograms have been bandpass-filtered (40–80 Hz) and amplitudes have been multiplied by a factor of $1/r^2$ for correction of the geometric spreading, where r is the distance between the source and stations. Arrows labeled with P1 and P1′ point the alignments of direct and refracted P waves from SP1 while arrows labeled with P2 and P2′ point the alignments of direct and refracted P waves from SP2. Arrivals of refracted P waves are denoted by solid dots in vertical-component seismograms. (*continued*)

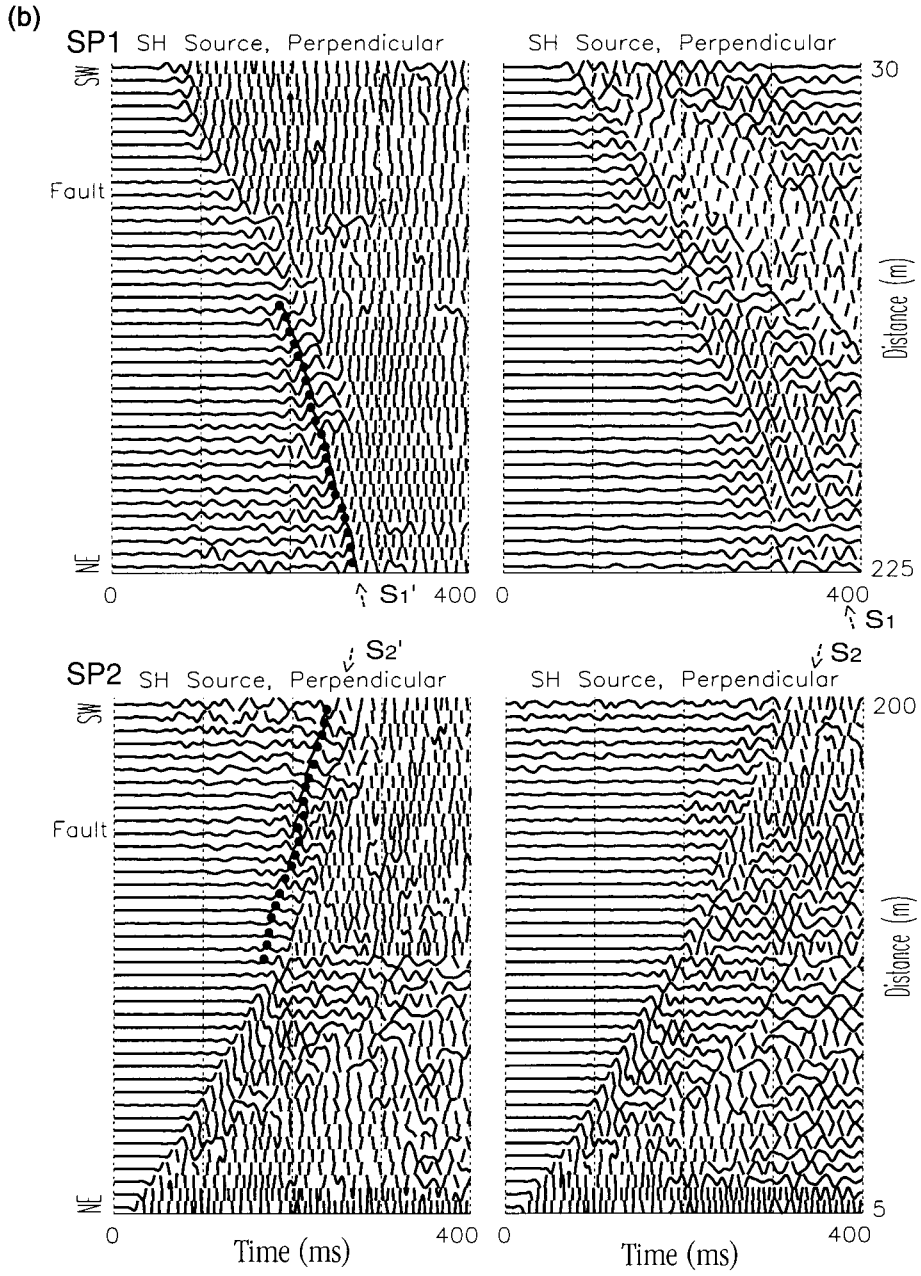

Figure 3. (*continued*) (b) Refraction profiles on a 195-m-long seismic array across the Punchbowl fault using the air-powered shear-wave source at source points (top) SP1 and (bottom) SP2, respectively. Perpendicular-to-array component seismograms are displayed. Seismograms in left panels have been bandpass-filtered (40–80 Hz) for showing refracted *SH* waves (labeled by S1′ and S2′) clearly while seismograms in right panels are bandpass-filtered (30–80 Hz) for showing direct *SH* waves (labeled by S1 and S2). Arrivals of *SH* waves are denoted by solid dots. Other notations are the same as in Figure 3a.

topography of the basement vary. After several iterations of raytracing inversion, we obtained the minimal root mean square (rms) travel-time residual of 1.55 msec for 229 *P* arrival-time measurements.

During modeling, we tested the effect of changing the position of the fault trace from the middle (0 m) of the model. When the fault was moved by 10 m from the middle, the rms travel-time residual for 229 *P* arrival-time measurements was 2.05 msec. When the fault was moved by a greater distance, the rms travel-time residual became larger. We also tested the model with a planar contact between the southwest granitic and the northeast sandstone blocks in bed-

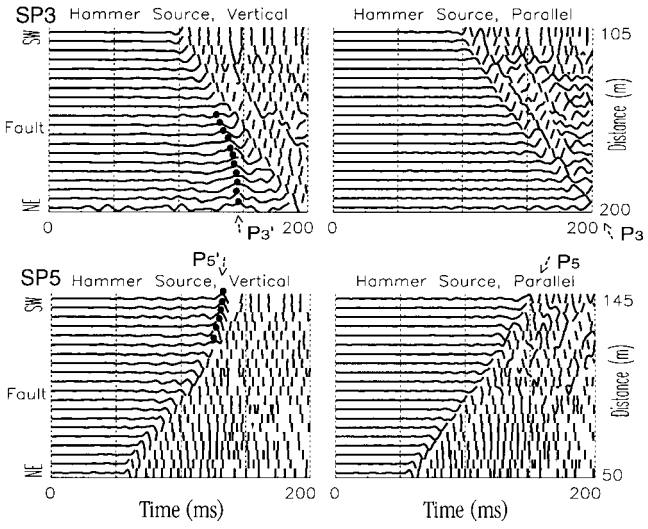

Figure 4. Refraction profiles on the southern half of seismic array across the Punchbowl fault using the hammer source at (top) SP3 and (bottom) SP5. Vertical and parallel-to-array component seismograms are displayed. Seismograms have been bandpass-filtered (40–80 Hz). Refracted *P* waves are denoted by solid dots. Other notations are the same as in Figure 3a.

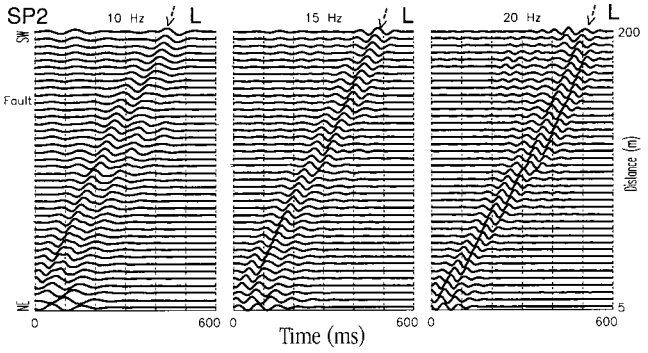

Figure 5. Multiple bandpass-filtered seismograms in profiles across the Punchbowl fault from for the *SH* source at SP2 using a filter with a 2-Hz band and centered at 10, 15, and 20 Hz. Seismograms are plotted using trace-normalized amplitude scale. Arrows labeled with L point the arrivals of energy of Love waves at the specific frequencies.

rock instead of a low-velocity fault zone sandwiched between them. Although the rms travel-time residual could be as small as that from the best fault-zone model, this model with a planar contact required a very high relief (~18 m) of the bedrock surface near the fault, which is not consistent with our observations of nearly straight alignment of refracted-wave arrivals in seismic profiles.

Because the Poisson's ratio was not adjustable in the existing inverse code, we tested the Poisson's ratio in a range of 0.2–0.4 by trial and error for *S*-wave modeling. When the Poisson's ratio was 0.25, the rms travel-time residual for 120 *S* arrival-time measurements had its minimum of 3.1 msec. As the Poisson's ratio increased, the travel-time residual became obviously larger.

The model parameters best fit to the data are shown in Figure 6a. The synthetic travel times for direct and refracted *P* and *S* waves using these model parameters are shown in Figures 6b and c, respectively, for a comparison with observations. Whereas the best-fit model in Figure 6a is not unique for raytracing inversion of *P*- and *S*-wave travel times from refraction profiling, this model is a simple, viable solution for the velocity structure of the Punchbowl fault zone. The fault is marked by a zone several tens of meters wide in which the velocity is reduced by 10%–25% from the wall-rock velocities, with the greatest reduction in the central part of the fault zone. The velocity of the crystalline wall rock southwest of the fault is higher than the velocity of the Punchbowl Formation sedimentary rock northeast of the fault. We interpret that the velocity reduction within the fault zone corresponds to the high crack density in the fault-zone rock. We further interpret that the cracks at shallow depth in the study area could be dry rather than wet because *S*-wave raytracing suggested an average Poisson's ratio of 0.25 for the rock near the fault, whereas we could not distinguish the Poisson's ratio within a narrow fault zone from wall rocks using the current raytracing code. In fact, water wells in this area show that the water table lies below the depths (~40 m) explored with the seismic refraction profile.

We computed the crack densities from the measured seismic velocities after using equations (5) to (8) of O'Connell and Budiansky (1974), in which the elastic constants of fractured rock are functions of the crack density. The crack density is defined by $\varepsilon = N\langle a^3\rangle/V$, where a is the radius of the flat penny-shaped crack and N is the number of cracks in volume V. Cracks were assumed to be dry and the Poisson's ratio was calculated to be 0.25. The effective shear modulus $\bar{\mu}$ is related to the crack density ε and the effective Poisson's ratio $\bar{\nu}$ by $\bar{\mu}/\mu = 1 - 32/45\,[(1-\bar{\nu})(5-\bar{\nu})/(2-\bar{\nu})]\,\varepsilon$, and $\lambda = \mu$ where λ and μ are Lame's constants of uncracked rock. We used $V_p = 3.8$ km/sec and $\rho = 2.4$ grams/cm^3 for the granitic and gneissic noncracked rock, and $V_p = 3.5$ km/sec and $\rho = 2.3$ grams/cm^3 for the noncracked sandstone of Punchbowl Formation. These values are constrained by the velocities measured in situ and in the laboratory. Hadley (1976) measured the velocity of nonfractured Westerly granite to be 4 km/sec under the confining pressure lower than several bars. Our refraction profiles sampled the basement rock at the depth of only several tens of meters at which the confining pressure is very low. V_p of 3.8 km/sec for the uncracked granitic bedrock at the shallow depth is a plausible value. Furthermore, small cores of the medium-grained sandstone of the Punchbowl Formation have a Young's Modulus of 17 GPa at a confining pressure of 50 MPa, which exerts enough pressure to close many of the microscopic grain-boundary fractures that are open at atmospheric pressure. For isotropy and Poissonian rock, a Young's modulus of 17 GPa implies a shear modulus

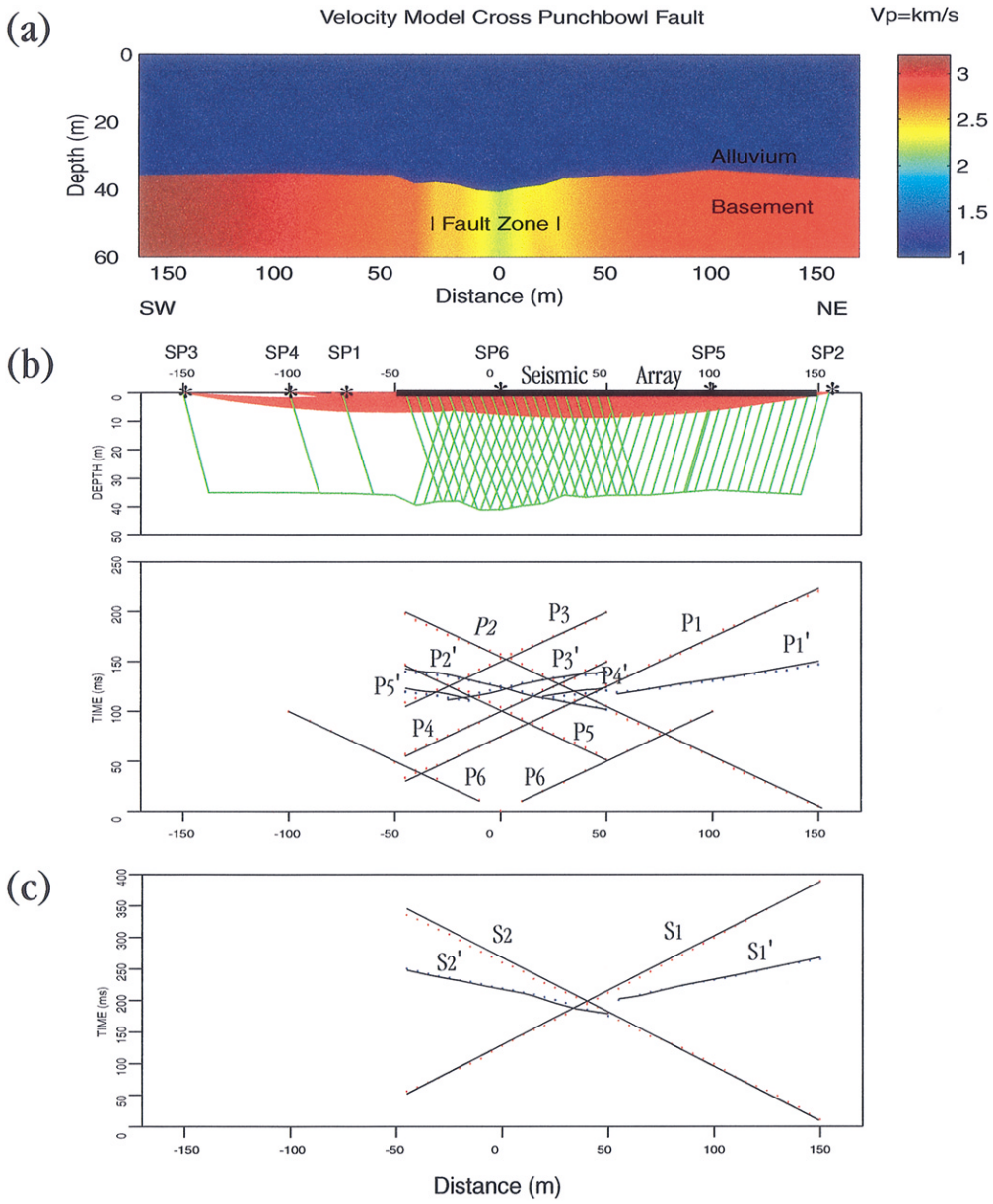

Figure 6. (a) The cross-fault V_p model for the Punchbowl fault zone. Model parameters obtained from the raytracing with inverse to best fit observed travel times of *P* and *S* waves. It is noted that this model has been rotated by 7° with respect to the ground surface and the realistic fault plane is not vertical in bedrock, but these differences do not affect the results of raytracing for shallow refraction profile. (b) Ray paths and synthetic travel times of direct (coded by the red color) and refracted (green) *P* waves from six source points (SP1-6) in refraction profiles across the Punchbowl fault using the best-fit *P*-wave model given in Figure 6a. Stars denote locations of source points. The thick solid line denotes the seismic array on ground surface. The interface between the alluvium and bedrock beneath the 195-m-long seismic array is covered by dense ray paths. Synthetic travel times are presented by thin lines and labeled by P or S with the subscript index corresponding to the source point number. The prime denotes the refracted wave. Observed travel times are presented by color dots. (c) Synthetic and observed travel times of direct and refracted *S* waves from two *SH* source points (SP1 and 2) in refraction profiles across the Punchbowl fault using the best-fit model given in Figure 6a and Poisson's ratio of 0.25. Other notations are the same as in Figure 6b but for *S* waves.

of 6.8 GPa, consistent with the velocity for the wall rock of Punchbowl Formation at the shallow depth.

The calculated crack densities near the Devil's Punchbowl fault are shown in Figure 7b, using the velocities measured from the seismic profile (Fig. 7a). The *P*-wave velocity at the center of the fault zone is 2.2 km/sec and increases to 3.2 km/sec in the granitic basement and 2.9 km/sec in the Punchbowl Formation at the distance of 150 m from the fault. The crack density decreases monotonically from the central high (~0.4) to the background value (~0.1) correspondingly. The increase in measured velocity and the decrease in calculated crack density from the center to the outer boundaries of the fault zone are approximately symmetric.

Discussions and Conclusions

The seismic velocity model in Figure 6a is consistent with our geologic subsurface model constructed on the basis of outcrop relations of the Punchbowl fault zone although the alluvial surface is actually inclined 7° to the north along the jeep trail, and the Punchbowl fault dips approximately 75° to the southwest. However, the geologic model (Fig. 2) indicates that the fault surface in bedrock at the 40-m depth is located at −10 m from the middle (0 m) of the velocity model where the velocity is lowest in the bedrock. The field observation has shown that fault-related damage is greatest at the ultracataclasite layer (Chester and Logan, 1986) so that the fault surface should correlate with the lowest velocity in the bedrock. The 10-m shift of the position of the fault surface between the geologic-based model and the seismic velocity model is probably caused by an error in the geologic-based location of the fault by the projection from the outcrops in the canyons 100 m away from the array site.

In the seismic velocity model (Fig. 6a), velocities decrease gradually from the values in the wall rocks to the lowest velocity centered on the fault, which is qualitatively similar to the gradual changes in deformation intensity measured as the fault surface is approached (Wilson *et al.,* 1999). If the velocity reduction is caused by fracturing, then the crack densities calculated from seismic velocities should have a pattern similar to the direct measurements of fracture density. Figure 7c shows a comparison of apparent crack densities determined from seismic velocities to measurements of microfracture density. The direct measurements show an extremely high fracture density within 1 m from the ultracataclasite layer. However, the seismic profiling cannot resolve velocity variation within such a narrow zone. Accordingly, we normalized both calculated crack densities and measured fracture densities by the value at a distance of 5 m from the fault surface. Overall, the calculated and measured fracture densities show similar variation with distance from the fault.

The low-velocity zones along active faults have generally been modeled as tabular zones with uniform velocity. On the basis of structural studies and the seismic velocity profile herein, a better model may be that of a tabular zone

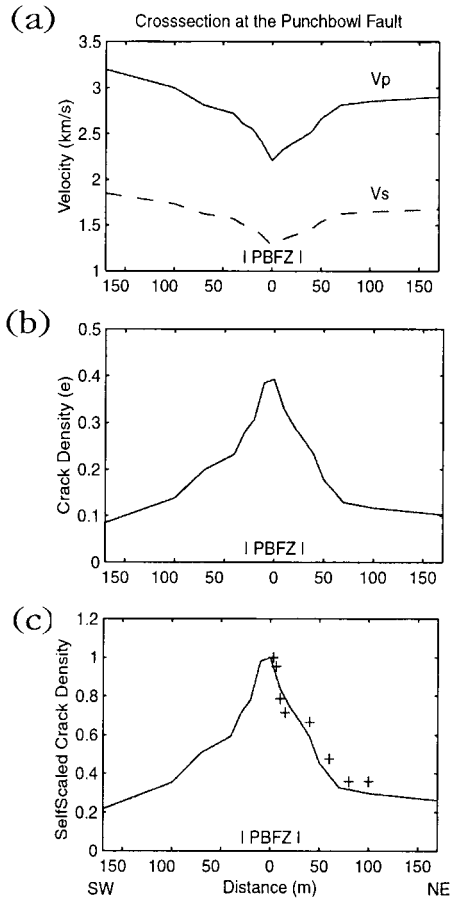

Figure 7. (a) *P* (solid line) and *S* (dotted line) velocities of bedrock measured from seismic refraction profiles across the Punchbowl fault zone. Velocities in the fault zone are reduced by 10%–25% from host-rock velocities, with the greatest reduction in the central part of the fault zone. (b) Crack densities calculated from measured seismic velocities using O'Connell and Budiansky (1974) analysis of a cracked medium. (c) Comparison of calculated crack density (line) and observed microfracture density (crosses) as a function of distance from the fault surface. Crack densities are normalized by the values at ±5 m. Microfracture densities in the sandstone of the Punchbowl Formation in the Devils Punchbowl are from Wilson *et al.* (1999).

with gradual reduction in velocity from the outer boundaries inward to a central velocity minimum (Fig. 7).

The studies of active faults using fault-zone trapped waves at Landers fault zone that ruptured in the *M* 7.5 earthquake of 1992 (Li *et al.,* 1999, 2000) have shown much greater magnitude reduction in velocity from wall rock to fault zone than that seen in the Punchbowl survey. We suggest that this difference may be attributed to the fact that the Punchbowl fault is inactive and some of the fractures are now healed. A greater proportion of fractures near the active faults are open, leading to greater reduction in fault-related velocity reduction, particularly just following major earth-

quakes, such as the Landers rupture zone, occurring on them. Postseismic fault healing has been observed in our repeated seismic surveys at the Landers rupture zone (Li *et al.,* 1998; Li and Vidale, 2001). We interpreted that the fault healing is most likely caused by the closure of cracks that were opened by the 1992 *M* 7.5 earthquake. At the Punchbowl fault zone, microstructural studies of the fault rocks reveal that many of the microfractures in the rocks have been completely healed and sealed (Chester and Logan, 1986). Many of the subsidiary faults are partially filled with cement. There is good structural evidence that fracturing and subsequent healing and sealing occurred throughout the Punchbowl faulting history (Wilson *et al.,* 1999).

In summary, (1) our seismic refraction profiling at the Punchbowl fault allowed us to delineate a low-velocity zone that is several tens of meters thick and that is sandwiched between the granitic and gneissic bedrock to the southwest and the Punchbowl Formation sandstone to the northeast. Within the fault zone, seismic velocities are reduced by 10%–25% from the host-rock velocities. As the velocity model from the inverse of raytracing for the travel times of seismic waves is not well constrained because of the uncertainties of fault geometry, alluvium depth, and bedrock topography, the model in Figure 6a is only one of the several possible interpretations for the data. Nonetheless, the seismic velocity model is admissible on the basis of structural and seismic data, and is the most plausible given the fracture fabric in the Punchbowl fault zone. (2) The thickness of the low-velocity zone and the gradual decreases in seismic velocity from the outer boundaries of the fault zone to the central velocity low is qualitatively consistent with expectations based on observations of fault-related damage. Crack-density profiles calculated from seismic velocity variation are consistent with direct measurements of microfracture density along traverses across the Punchbowl fault zone. (3) The seismic velocity and fracture density distributions of the Devil's Punchbowl fault zone suggest that the fracturing is a major deformation feature in the damaged zone of the Punchbowl fault and increases with proximity to the fault core. These results encourage us to use seismic methods to image fault damage zones and characterize geometric complexity of fault zones at depth.

Acknowledgments

This research was supported by the Southern California Earthquake Center. SCEC is funded by NSF Cooperative Agreement EAR-8920136 and USGS Cooperative Agreements 14-08-0001-A0899 and 1434-HQ-97AG01718. The IRIS-PASSCAL Instrument Center provided their seismic recording for this research project. We are indebted to Hsi-Ping Liu of the U.S. Geological Survey for kindly offering the shear-wave source used in our experiment. We acknowledge Hsi-Ping Liu and Fei Xu of UCLA for their work in the field. We used the RAYINVR code of Colin Zelt in modeling. We thank David Numer and Jack Farley of the Devil's Punchbowl Los Angeles County Park for their assistance. In addition, the homeowners in the Punchbowl area are thanked for their patience with our field activities. Reviews from Editor Mike Fehler, reviewer Susan Hough, and an anonymous reviewer improved the manuscript.

References

Aki, K., and W. H. K. Lee (1976). Determination of three-dimensional velocity anomalies under a seismic array using first *P* arrival times from local earthquakes, 1, a homogeneous initial model, *J. Geophys. Res.* **81,** 4381–4399.

Chester, F. M., and J. S. Chester (1998). Ultracataclasite structure and friction processes of the Punchbowl fault, San Andreas system, California, *Tectonophysics* **295,** 199–221.

Chester, F. M., and J. M. Logan (1986). Implications for mechanical properties of brittle faults from observations of the Punchbowl fault zone, California, in *Internal Structure of Fault Zone,* C.-Y. Wang (Editor), *Pure Appl. Geophys.* **124,** 79–106.

Chester, F. M., and J. M. Logan (1987). Composite planar fabric of gouge from the Punchbowl fault, California, *J. Struct. Geol.* **9,** 621–634.

Chester, F. M., J. P. Evans, and R. L. Biegel (1993). Internal structure and weakening mechanisms of the San Andreas fault, *J. Geophys. Res.* **98,** 771–786.

Cox, B. F., R. E. Powell, M. E. Hinkle, and D. A. Lipton (1983). Mineral resource potential map of the Pleasant View Roadless Area, Los Angeles County, California. U.S. Geol. Surv. Misc. Field Stud. Map MF-1649-A, scale 1:62,500.

Dibblee, T. W. Jr. (1968). Displacements of the San Andreas fault system in the San Gabriel, San Bernardino, and San Jacinto Mountains, southern California, in *Proceedings of the Conference on Geological Problems of the San Andreas fault system,* Stanford Univ. Publ. Geol. Sci., Stanford, California, Vol. 11, 260–276.

Dibblee, T. W. Jr. (1987). Geology of the Devil's Punchbowl, Los Angeles County Park, California, Geol. Am. Centennial Field Guide-Cordilleran Section, 207–210.

Eberhart-Phillips, D., and A. J. Michael (1993). Three-dimensional velocity structure, seismicity, and fault structure in the Parkfield region, central California, *J. Geophys. Res.* **98,** 15,737–15,758.

Hadley, K. (1976). Comparison of calculated and observed crack densities and seismic velocities in westerly granite, *J. Geophys. Res.* **81,** 3484–3494.

Hough, S. E., Y. Ben-Zion, and P. Leary (1994). Fault-zone waves observed at the southern Joshua Tree earthquake rupture zone, *Bull. Seism. Soc. Am.* **84,** 761–767.

Johnson, A. M., R. W. Fleming, and K. M. Cruikshank (1994). Shear zones formed along long, straight traces of fault zones during the 28 June 1992 Landers, California, earthquake, *Bull. Seism. Soc. Am.* **84,** 499–510.

Leary, P. C., H. Igel, and Y. Ben-Zion (1991). Observation and modeling of fault zone seismic trapped waves in aid of precise precursory microearthquake location and evaluation, in *Proc. Conf. Earthquake Prediction: State-of-the Art,* Strasbourg, France, 15–18 October 1991.

Lees, J. M., and P. E. Malin (1990). Tomographic images of *P* wave velocity variation at Parkfield, California, *J. Geophys. Res.* **95,** 21,793–21,804.

Li, Y. G., and J. E. Vidale (2001). Healing of the shallow fault zone from 1994–1998 after the 1992 *M* 7.5 Landers, California, earthquake, *Geophys. Res. Lett.* **28,** 2999–3002.

Li, Y. G., P. C. Leary, K. Aki, and P. E. Malin (1990). Seismic trapped modes in the Oroville and San Andreas fault zones, *Science* **249,** 763–766.

Li, Y. G., J. E. Vidale, K. Aki, C. J. Marone, and W. H. K. Lee (1994). Fine structure of the Landers fault zone: segmentation and the rupture process, *Science* **256,** 367–370.

Li, Y. G., K. Aki, J. E. Vidale, and F. Xu (1999). Shallow structure of the Landers fault zone from explosion-generated trapped waves. *J. Geophys. Res.* **104,** 20,257–20,275.

Li, Y. G., J. E. Vidale, K. Aki, and F. Xu (2000). Depth-dependent structure of the Landers fault zone from trapped waves generated by aftershocks, *J. Geophys. Res.* **105,** 6237–6254.

Li, Y. G., J. E. Vidale, K. Aki, F. Xu, and T. Burdette (1998). Evidence of

shallow fault zone strengthening after the 1992 M7.5 Landers, California, earthquake. *Science* **279,** 217–219.

Liu, H. P., R. L. Maier, and R. E. Warrick (1996). An improved air-powered impulsive shear-wave source, *Bull. Seism. Soc. Am.* **86,** 530–537.

Michelini, A., and T. V. McEvilly (1991). Seismological studies at Parkfield, I, simultaneous inversion for velocity structure and hypocenters using cubic B-splines parameterization, *Bull. Seism. Soc. Am.* **81,** 524–552.

Mooney, W. D., and A. Ginzburg (1986). Seismic measurements of the internal properties of fault zones, *Pure Appl. Geophys.* **124,** 141–157.

O'Connell, R. J., and B. Budiansky (1974). Seismic velocities in dry and saturated cracked solids, *J. Geophys. Res.* **79,** 5412–5426.

Schulz, S. E., and J. P. Evans (1998). Spatial variability in microscopic deformation and composition of the Punchbowl fault, southern California: implications for mechanisms, fluid-rock interaction, and fault morphology, *Tectonophysics* **295,** 223–244.

Sibson, R. H. (1977). Fault rocks and fault mechanisms, *J. Geol. Soc. Lond.* **133,** 191–213.

Sieh, K., L. Jones, E. Hauksson, K. Hudnut, D. Eberhart-Phillips, T. Heaton, S. Hough, K. Hutton, H. Kanamori, A. Lilji, S. Lindvall, S. McGill, J. Mori, C. Rubin, J. Spotila, J. Stock, H. Thio, J. Treiman, B. Wernick, and J. Zachariasen (1993). Near-field investigations of the Landers earthquake sequence, April to July 1992, *Science* **260,** 171–176.

Thurber, C. H. (1983). Earthquake locations and three-dimensional crustal structure in the Coyote Lake area, central California, *J. Geophys. Res.* **88,** 8226–8236.

Weldon, R. J. II, K. E. Meisling, and J. Alexander (1993). A speculative history of the San Andreas fault in the central Transverse Ranges, California, in *The San Andreas Fault System: Displacement, Palinspastic Reconstruction, and Geological Evolution,* R. E. Powell, R. J. Weldon, II, and J. C. Matti (Editors), Geol. Soc. Am. Memoir, Vol. 178, 161–198.

Wilson, J. E., J. S. Chester, and F. M. Chester (1999). Microfracture fabric of the Punchbowl fault zone, San Andreas system, California, *EOS Trans. AGU* **80,** F746.

Zelt, C. A., and R. B. Smith (1992). Seismic traveltime inversion for 2-D crustal velocity structure, *Geophys. J. Int.* **108,** 16–34.

Department of Earth Sciences
University of Southern California
Los Angeles, California 90089-0740
ygli@terra.usc.edu
(Y.-G. L.)

Department of Geology and Geophysics
Texas A&M University
College Station, Texas 77843-3115
(F.M.C.)

Department of Earth and Space Sciences
University of California, Los Angeles
Los Angeles, California 90095-1567
(J.E.V.)

Manuscript received 31 March 2000.